https://doi.org/10.5194/tc-2021-381
Preprint. Discussion started: 4 January 2022

The Cryosphere Discussions

Antarctic sea ice types from active and passive microwave remote sensing

Christian Melsheimer[1], Gunnar Spreen[1], Yufang Ye[2], and Mohammed Shokr[3]

[1]Institute of Environmental Physics (IUP), University of Bremen, Germany
[2]School of Geospatial Engineering and Science, Sun Yat-Sen University, Zhuhai, China
[3]Environment and Climate Change Canada, Toronto, Canada

Correspondence: Christian Melsheimer (melsheimer@uni-bremen.de)

Abstract.

Polar sea ice is one of the Earth's climate components that has been significantly affected by the recent trend of global warming. While the sea ice area in the Arctic has been decreasing at a rate of about 4% per decade, the multi-year ice (MYI), also called perennial ice, is decreasing at a faster rate of 10%–15% per decade. On the other hand, the sea ice area in the Antarctic region was slowly increasing at a rate of about 1.5% per decade until 2014 and since then it has fluctuated without a clear trend. However, no data about ice type areas are available from that region, particularly of MYI. Due to differences in physical and crystalline structural properties of sea ice and snow between the two polar regions, it has become difficult to identify ice types in the Antarctic. Until recently, no method has existed to monitor the distribution and temporal development of Antarctic ice types, particularly MYI throughout the freezing season and on decadal time scales. In this study, we have adapted a method for retrieving Arctic sea ice types and partial concentrations using microwave satellite observations to fit the Antarctic sea ice conditions. The first circumpolar, long-term time series of Antarctic sea ice types; MYI, first-year ice and young ice is being established, so far covering years 2013-2019. Qualitative comparison with synthetic aperture radar data, with charts of the development stage of the sea ice, and with Antarctic polynya distribution data show that the retrieved ice types, in particular the MYI, are reasonable. Although there are still some shortcomings, the new retrieval for the first time allows insight into the evolution and dynamics of Antarctic sea ice types. The current time series can in principle be extended backwards to start in the year 2002 and can be continued with current and future sensors.

1 Introduction

As an important component of the global climate system, sea ice affects and reflects changes in other climate components, controls energy and gas fluxes between ocean and atmosphere in polar regions, and it is an important part of the polar marine ecosystem. The Arctic sea ice extent has decreased by 4.1% per decade in the past three decades (Parkinson and Cavalieri, 2012b), while the declining rate for multiyear ice (MYI), ice that has survived at least one summer melt, is much higher,

https://doi.org/10.5194/tc-2021-381
Preprint. Discussion started: 4 January 2022

10–15% per decade (Johannessen et al., 1999; Comiso, 2012; Meredith et al., 2019). This ice, which is also called perennial ice, is the counterpart of seasonal ice which is defined as ice that forms in the beginning of freezing season and melts in the following summer. It includes young ice (YI), which has thickness less than 30 cm and the more common first-year ice (FYI), which is thicker than 30 cm. Three decades ago, MYI covered two thirds of the Arctic Basin. This portion has dropped to one third recently and the MYI has been replaced by FYI (Kwok et al., 2009).

In contrast to Arctic ice, sea ice extent in the Antarctic has increased by 1.5% per decade since the 1970s until 2014 (Parkinson and Cavalieri, 2012a). Since then, it has strongly decreased and than partly rebounded, so it is too early to quantify any new trend (cf. Ludescher et al., 2019; Parkinson, 2019). Only a small fraction of the sea ice in the Antarctic survives the summer and hence becomes MYI; it is mostly found in the Weddell Sea, but also on the Western side of the Antarctic Peninsula and in small patches around the coast (Stocker et al., 2013).

Almost all MYI in the Antarctic is in fact second-year ice (SYI) but it is difficult to discriminate between SYI and older ice using satellite data. For the remainder of this study, the term MYI usually denotes Antarctic second year ice. Unlike the Arctic, the evolution and spatial distribution of sea ice types in the Antarctic are still unclear. The MYI area of the Antarctic may have followed an increasing trend, based on the fact that in the Austral summer the sea ice extent of the Antarctic has increased by 3.6% per decade from 1979 to 2010 (Parkinson and Cavalieri, 2012a). As this is the sea ice which is becoming MYI one can assume that the MYI area overall increased at a similar rate. Antarctic sea ice has strong region-dependent effects on ecosystem structure and function (Massom and Stammerjohn, 2010). In the absence of information on the sea ice type distribution and evolution, the ice mass balance and the energy fluxes between ocean and atmosphere are still unknown. MYI also is a good proxy for the total ice and snow thickness and thereby the MYI distribution influences energy fluxes and serves as an indicator or response to climate forcing.

Sea ice cover, and particularly MYI in the Antarctic, is different in many ways from Arctic ice. There is commonly a thicker snow cover, which may cause the underlying sea ice to be depressed below the water surface and thus be flooded, creating so-called flooded ice, and, when refreezing, snow ice. In addition, water from partial snow melt that percolates down and refreezes at the bottom of the snow layer forms so-called superimposed ice, which is more common in the Antarctic than in the Arctic (Haas et al., 2001). The ice cover in the Antarctic is also rougher than that in the Arctic because it is exposed to higher wind that triggers more motion and collisions between ice floes. The turbulent ocean water leads to formation of frazil ice crystalline structure, which is another difference compared to the mostly congealed structure of the Arctic sea ice For these reasons, statistical distributions of radiometric and backscattering observations are different between the two regions.

Most of the Antarctic MYI is found in the Weddell Sea. The Weddell Gyre transports the MYI away from the coast (where it has survived the summer), towards the north-western and northern Weddell Sea. Spatial and temporal observations of the MYI distribution are needed to better understand these processes. Beside MYI, the other ice types are of interest as well. Along the costs large landfast ice areas develop regularly (Nihashi and Ohshima, 2015). In polynyas, new and YI types alter the mass balance and surfaces fluxes. In the marginal ice zone (MIZ), pancake ice can form, and ice floes are smaller and more deformed due to the influence of wind and waves. Monitoring the dynamic and vast sea ice cover requires satellite observations. A physically consistent time series of sea ice types is needed to ascertain trends and quantify the interaction of sea ice within

https://doi.org/10.5194/tc-2021-381
Preprint. Discussion started: 4 January 2022

the climate system. Currently, climate models are not yet able to correctly reproduce realistic future scenarios of the Antarctic sea ice extent and especially regional patterns are not well reproduced (Mahlstein et al., 2013; Polvani and Smith, 2013; Hobbs et al., 2015; Turner et al., 2015; Zunz et al., 2013). In order to improve and better validate climate models, time series with more detailed information about the sea ice types are required.

Total and partial sea ice concentration (i.e., the area fraction of ice, in per cent, within an observation cell) can be estimated from microwave satellite observations because in this spectral range different ice types have different emission and scattering properties. Recently, a method has been developed to estimate partial and total concentration of Arctic ice types using a combination of active and passive microwave satellite measurements (i.e., from scatterometer and radiometer, respectively) and additional ancillary data of air temperature and ice drift vectors. The method is based on Environment Canada's Ice Concentration Extractor algorithm, ECICE (Shokr et al., 2008; Shokr and Agnew, 2013) and a later modification to account for anomalies incurred as a result of possible warm spells during transition seasons, which causes the microwave signal to generate from the wet snow cover instead of the underlying sea ice. The modification uses surface temperature from meteorological reanalysis and ice drift from satellite data in order to correct misclassifications caused by melt-refreeze cycles and by snow metamorphosis. This has been successfully applied and tested in the Arctic (Ye et al., 2016a, b) and has recently also been compared to other sea ice type retrieval results (Ye et al., 2019). In this study, we have adapted this method to the Antarctic conditions with the aim of eventually filling the data gap in the Antarctic – the lack of ice type, in particular, multiyear ice, data. The only other approach of regularly retrieving sea ice type in the entire Antarctic from remote sensing data is the ice type classification based on microwave radiometer data, recently (summer 2021) released by the Ocean and Sea Ice Satellite Application Facility (OSI-SAF) (Aaboe et al., 2021a).

This paper is organised as follows: In Section 2 we give a brief account of ECICE and its adaptation to the Antarctic conditions. In Section 3, the first results, of the Antarctic sea ice type concentration mapping spanning the years 2013 to date are compared with results from Sentinel-1 radar images, an existing a ice chart data set of the stage of development of sea ice and another data set of polynyas. In Section 4, we discuss remaining problems and shortcomings, and Section 5 presents a summary and conclusions.

2 Estimation of Sea Ice Type Concentration

Satellite-based estimation of the total ice concentration and of partial concentration of different ice types like MYI, FYI and YI can be obtained using the Environment Canada's Ice Concentration Extractor (ECICE). It takes input from any set of satellite observations and produces concentrations of any given ice types (Shokr et al., 2008). Our estimation of MYI concentration actually is a two-step procedure that first uses ECICE and then applies two correction schemes to the output MYI concentration in order to account for anomalies of the observations (Ye et al., 2016a, b). One anomaly causes misclassification of MYI as FYI (usually observed in autumn) and the other causes misclassification of FYI as MYI (usually observed in spring).

https://doi.org/10.5194/tc-2021-381
Preprint. Discussion started: 4 January 2022

2.1 ECICE – Environment Canada's Ice Concentration Extractor

ECICE can take passive and active microwave satellite measurements as input. Possible passive microwave input data are from the satellite microwave radiometers Special Sensor Microwave/Imager (SSM/I, 1987-2009), Advanced Microwave Scanning Radiometer for EOS (AMSR-E, 2002-2011) and Advanced Microwave Scanning Radiometer 2 (AMSR2, 2012-present). The measured quantities are the brightness temperatures at different frequencies and at vertical (V) as well as horizontal (H) polarisation. Possible active microwave input data include scatterometer measurements from QuikSCAT (1999-2009) and Advanced Scatterometer (ASCAT, 2007-present). The measured quantity is the backscattering coefficient (normalised radar backscattering cross section) at one or two polarisations (HH and VV). The number of input parameters to ECICE must be equal or greater than the number of the surface types to be distinguished. Here we use four surface types; namely open water, young ice (YI), first-year ice (FYI), and multiyear ice (MYI). The input parameters are listed in Table 1 and explained in Section 2.3.

Most methods that retrieve the concentration of sea ice or sea ice types from radiometer or radar data use representative values of each input parameter for each surface type (ice or ice types, open water) – these representative values are known as tie points. In contrast, ECICE uses the statistical distribution of all possible values of each input parameter for each surface type. Such distributions are obtained by sampling data of the given input parameter from the given surface obtained under different meteorological, dynamic and freezing conditions. The distributions have been established for the application of Arctic sea ice (Shokr et al., 2008; Ye et al., 2016a) and re-established here for the Antarctic application (see details in Section 2.3). With the distributions, which can be interpreted as probability densities, a number n of possible realisations of tie points for all surfaces is selected using a random number generator. Here, we use 1000 realisations. For any given observation in remote sensing data, the observation is considered to represent a linear mixture of typical values (tie points) for of each surface type, weighted by the area fraction of that surface type in the observation cell. Therefore, a set of linear equations (equal to the number of observations) in which each equation represents decompositions of each input observation into its components from the given surface types is then constructed. The equations are solved simultaneously for the area fraction of each surface type under the constraint that all fractions must add up to one (equality constraint) and that each area fraction must be between 0 and 1 (inequality constraint). This formulates the problem into an inequality constrained optimisation problem, which is solved to find the ice concentrations that minimise a given coast function. Then, the median of the n solutions for the area fractions (i.e., concentrations) is produced from which the final answer is generated (a set of concentrations of the given ice types). In addition, the spread of the n solutions around the median is used as a measure of confidence of the result for each surface type (Shokr et al., 2008).

2.2 Correction schemes

The determination of the ice type concentrations (i.e., the area fractions of the three ice types) is only based on their radiometric and backscattering properties. During atmospheric warm spells, commonly occurring in the transition seasons, snow wetness develops. The return of cold temperatures may cause snow metamorphism. Both effects cause anomalous microwave

https://doi.org/10.5194/tc-2021-381
Preprint. Discussion started: 4 January 2022

observations that make MYI appear as FYI and vice versa. Another process that causes anomalous observations is ice surface deformation at floe edges (e.g., pancake ice), which makes brightness temperature and backscattering from FYI look similar to those from MYI. Such errors are reduced by the two corrections schemes described in the following sections.

2.2.1 Temperature Correction

Warm air advection can occur during fall and spring seasons. When air temperature rises to near melting or beyond melting conditions, snow wetness develops and MYI will have lower backscatter and higher brightness temperature, typical of FYI. Therefore, it is misclassified by ECICE as FYI (more precisely: the retrieved MYI concentration is too low and the FYI concentration too high). After the end of the warm event, which typically takes between one to a few days, the correct classification is resumed. In order to account for this error, the so-called temperature correction scheme (Ye et al., 2016a) examines the 2-m air temperature (T2m) data to identify warm episodes of up to N days. Each episode starts with temperatures rising above a threshold T_1 (near freezing temperature) and ends with temperatures falling below a threshold T_2. If the MYI concentration drops at any location during a warm spell by more than a specified threshold ΔC_t and later rises again, such MYI concentrations are replaced by values linearly interpolated from before and after the warm episode. The values of the parameters N, T_1, T_2 and ΔC_t used here are specified in Section 2.3 (Table 2).

2.2.2 Drift Correction

Since the warm temperatures in the spring may progress for the rest of the season, the above temperature correction may not hold because it depends on the returning to the normal cold winter temperatures. For this reason, another correction was developed to identify locations of estimated MYI which are not realistic. This correction is based on the fact that MYI starts by definition as all remaining ice at the end of the melting season, i.e., at the onset of freeze-up. After that, MYI can only drift and its concentration can only be changed by divergence, convergence, and melting, but it cannot be generated during the cold season. Therefore, MYI is unrealistic if it appears at locations to which it cannot have drifted. To identify such locations, daily ice drift data are used to implement what is called "drift correction" (Ye et al., 2016b). This correction starts with defining the boundary of MYI cover from the map of a given day. The boundary is then adjusted according to the ice drift map of the same day to predict its contour in the next day. This is done by applying ice motion vectors (obtained from the sources mentioned below) to all pixels inside the boundary. This domain is then further extended by one grid cell to the outside in order to account for uncertainty of the ice drift product. Any MYI that has been retrieved outside of this domain cannot be multiyear ice. Therefore, all non-zero MYI concentrations in grid cells outside the mentioned domain are set to zero. However, since this spurious/erroneous MYI is in fact FYI or YI that has anomalous radiometric and scattering properties (so that ECICE has classified it as MYI), it is kept as a new pseudo-ice-type, which we call Ex-MYI. In addition, this correction scheme includes correction for some effects of snow metamorphosis for pixels inside the MYI contour of the given day which would make FYI radiometrically similar to MYI. It looks for sudden (within one day) rises ΔC_d of MYI concentration concurrent with sudden reductions of ΔT_{37} of $T_{B,37\mathsf{V}}$ or reductions ΔT_{19-37} of $T_{B,19\mathsf{H}} - T_{B,37\mathsf{H}}$. The latter difference is also called horizontal range, HR, and is used by Drobot and Anderson (2001) to identify the onset of snow melt. The use of this parameter in the drift

https://doi.org/10.5194/tc-2021-381
Preprint. Discussion started: 4 January 2022


The Cryosphere Discussions
Open Access
EGU

Instrument	Parameter	Frequ. [GHz]	Polarisation
AMSR2	T_B	37	V
AMSR2	T_B	37	H
AMSR2	GR	19, 37	V
ASCAT	σ°	5.3	VV

Table 1. Input parameters ("channels") used in Antarctic sea ice type retrieval with ECICE. Note: T_B is brightness temperature, GR is gradient ratio (see Equation (1)), σ° is normalised radar backscattering cross section.

155 correction is explained in detail in Ye et al. (2016b). In cases of such anomalies, the MYI concentration at the given pixel is replaced by the value of the previous day. The values of the parameters ΔC_d, ΔT_{37}, and ΔT_{19-37} used here are specified in Section 2.3 (Table 3).

2.3 Adapting ECICE algorithm to the Antarctic sea ice

The Antarctic implementation of ECICE at the Institute of Environmental Physics (IUP) at the University of Bremen uses as
160 input microwave radiometer data of the sensors AMSR-E (Advanced Microwave Scanning Radiometer for EOS) on the NASA satellite Aqua (2002–2011), or AMSR2 (Advanced Microwave Scanning Radiometer 2) on the JAXA satellite GCOM-W1 (since 2012), and scatterometer data from ASCAT (Advanced Scatterometer) on the European polar-orbiting satellites MetOp-A and MetOp-B. The input parameters ("channels") we use are the same as for the Arctic sea ice type retrieval (Ye et al., 2016a, b), they are listed in Table 1. The gradient ratio at 19 and 37 GHz, V polarisation is defined as

165 $$GR(37V, 19V) = \frac{T_{B,37\mathrm{V}} - T_{B,19\mathrm{V}}}{T_{B,37\mathrm{V}} + T_{B,19\mathrm{V}}} \quad (1)$$

For all input parameters, we use daily gridded data, projected on a polar stereographic grid with a nominal resolution of 12.5 km. This is the common grid used by the National Snow and Ice Data Center, NSIDC (see more details in Melsheimer and Spreen, 2019). The grid spacing is close to the resolution and the sampling interval of the original swath data of the used AMSR2 channels.

170 As Antarctic sea ice is different from Arctic sea ice (see Section 1), the probability distributions of the input parameters needed by ECICE for the Antarctic application had to be derived. The three ice types are MYI, first-year ice (FYI), and young ice (YI), i.e., ice that has just formed and is less than about 30 cm thick. The sample areas from which the distributions were derived were chosen as follows: For FYI and MYI, we used the time evolution of total sea ice from the operational ASI sea ice concentration retrieval in the year 2018[1]: At the beginning of the cold season, all remaining ice (mainly in the Weddell
175 Sea) is MYI by definition. Later in the season, sea ice that has formed in the season away from the MYI is FYI. For reliable samples of YI, we have used a satellite-based polynya data set from 2018 which is based on the Polynya Signature Simulation Method (PSSM, Markus and Burns, 1995) in the implementation by Kern et al. (2007), using combinations of the 36 GHz and 85 GHz, H and V polarisation channels of the Special Sensor Microwave/Imager (SSM/I). The data contain a surface class

[1] ARTIST Sea Ice (ASI) algorithm (Spreen et al., 2008) https://seaice.uni-bremen.de/sea-ice-concentration/, Melsheimer and Spreen (2019)

https://doi.org/10.5194/tc-2021-381
Preprint. Discussion started: 4 January 2022


The Cryosphere Discussions

Table 2. Parameter setting for the **temperature correction** scheme

Parameter	Meaning	Value
T_1	thresh. temp., start of warm episode	-1°C
T_2	thresh. temp., end of warm episode	2°C
N	max. duration of warm episode	10 days
ΔC_t	min. drop of MYI conc.	10%

Table 3. Parameter setting for the **drift correction** scheme

Parameter	Meaning	Value
ΔC_d	min. rise of MYI conc.	20%
ΔT_{37}	min. drop of $T_{B,37\mathrm{H}}$	20 K
ΔT_{19-37}	min. drop of $T_{B,19\mathrm{H}} - T_{B,37\mathrm{H}}$	10 K

"thin ice", which was used here for YI. For the surface class "open water", sample areas in the Southern Ocean in August 2018 and in the ice-free part of the Ross Sea in March 2018 were taken. The distribution functions of the four input parameters for the surface types YI, FYI, MYI and open water are shown in Figure 1. It is obvious that the four surface types cannot be distinguished using a single input channel, as the distributions generally overlap. However in some channels one specific surface type has a peak separated from the others, e.g., the backscatter (σ°) from MYI (Figure 1, top left panel, red curve), or GR(37V,19V) of OW (bottom left panel, blue curve). In addition, there are pairs of mutually non-overlapping distributions, such as OW and YI for T_B(37V) (top right panel, blue and cyan curves), or OW and FYI for T_B(37H) (bottom right panel, blue and green curves).

For the correction schemes, we use surface temperature data from meteorological reanalysis of the European Centre for Medium-Range Weather Forecast (ECMWF), namely, from the ERA Interim data set (Dee, 2011), and the low resolution sea ice drift product of the EUMETSAT Ocean and Sea Ice Satellite Application Facility (OSI SAF, www.osi-saf.org, Lavergne et al., 2010). Note that sea ice motion data from the National Snow and Ice Data Center (NSIDC) (Tschudi et al., 2016) can also be used. The used values of the temperature correction parameters, N, T_1, T_2, ΔC_t (Section 2.2.1) are listed in Table 2, and the used values of the drift correction parameters, ΔC_d, ΔT_{19-37}, and $T_{B,19\mathrm{H}}$ (see Section 2.2.2) are listed in Table 3.

The final result of the two-step retrieval scheme are MYI map data. In addition, as an intermediate result, a preliminary distinction of the sea ice into three types, i.e., MYI, FYI and YI (without applying any correction) is produced as well. Hereinafter it is called "uncorrected YI, FYI, MYI concentration".

To date, we have retrieved data for the cold seasons 2013-2020. For each year, we have retrieved the ice type concentrations for the months of February to November (autumn, winter and spring). As the correction schemes need extra time to check for transient changes in MYI concentration and temporary warming events, the corrected MYI concentration is available from

https://doi.org/10.5194/tc-2021-381
Preprint. Discussion started: 4 January 2022

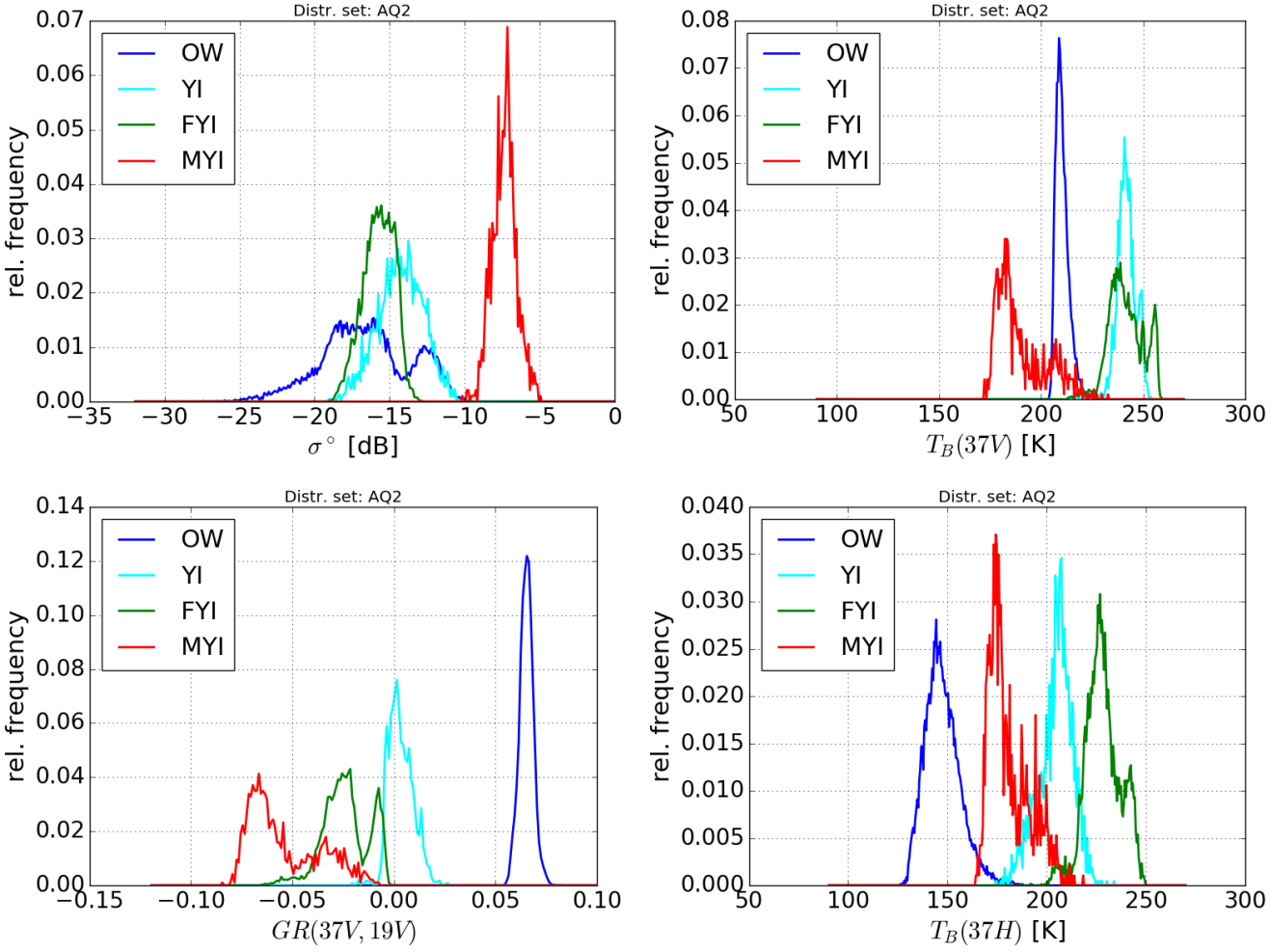

Figure 1. Distribution of the four input parameters to ECICE for the Antarctic surface types of MYI (red), FYI (green), YI (cyan) and open water (blue): ASCAT σ°(top left), AMSR2 T_B at 37 GHz, V polarisation (top right); AMSR2 T_B at 37 GHz, H polarisation (bottom right), and AMSR2 GR(37V,19V) (bottom left).

22 February to 8 November each year (roughly the Antarctic freezing season) – see the example for YI, FYI and corrected MYI in Section 3.2 (Figure 3).

Note that retrieving Antarctic ice types in the freezing seasons of 2002-2011 is possible, using AMSR-E instead of AMSR2, and QuikSCAT instead of ASCAT before 2008. For the years before 2013 (start of OSISAF drift data record for Antarctic), the sea ice drift data needed for the correction scheme of the MYI concentration are available from NSIDC.

https://doi.org/10.5194/tc-2021-381
Preprint. Discussion started: 4 January 2022

3 Comparison with other data

Validation of sea ice type concentration is a challenging task not only because there are few in-situ data sets of ice types available for the Antarctic region but also because point observations do not represent the large footprints of the satellite data. Validation studies using data from research cruises in the Antarctic have just started recently.

In this study we have compared the sea ice type concentration output from ECICE against three related satellite-based data sets: The new Antarctic uncorrected FYI and YI data and the corrected MYI data have been compared to data from (1) synthetic aperture radar (SAR) images, (2) charts showing the stage of development (SoD) of the ice, (3) maps of thin ice from the polynya data set mentioned above. Examples are presented in the following.

3.1 Synthetic Aperture Radar (SAR) Images

The MYI concentration from ECICE has been checked against high resolution SAR images acquired by Sentinel-1A/B at 40 m grid resolution. In SAR images, MYI usually looks considerably brighter than FYI and YI mainly because of the high backscatter triggered by volume scattering from the bubbly sub-surface layer. We have examined a few cases in the Weddell Sea and near the Antarctic Peninsula. An example is presented in Figure 2, showing an area in the Weddell Sea on 11 Aug, 2016. The Sentinel-1 SAR image (grey shade) is overlaid on the MYI concentration (colour scale). In addition, the dominant ice type is indicated by the coloured contours; white: YI=50%; purple: FYI=70%; black: MYI=70%.

The black and purple contours, which mark the transition from MYI to FYI, coincide well with a clear boundary between bright and dark radar backscatter which marks the boundary between dominating MYI and dominating FYI. Note also that ECICE correctly identifies an area of YI in the lee of the grounded iceberg A23A. However, the iceberg itself is erroneously retrieved as FYI. Qualitatively, the comparison to the other Sentinel-1 scenes is similarly good.

3.2 Stage of Development (SoD) Charts

Weekly charts of the stage of development (SoD) of the Antarctic sea ice have been jointly produced by the U.S. National Ice Center (NIC), the Russian Arctic and Antarctic Research Institute (AARI) and the Ice Service of the Norwegian Meteorological Institute (NIS) since December 2014 (*AARI-NIC-NMI pilot project on integrated sea ice analysis for Antarctic waters*, http://ice.aari.aq/antice/). The charts, based on analysis of visible/infrared and microwave satellite imagery and reconnaissance data by experienced specialists, show various ice types, grouped roughly into YI, FYI, MYI. In this classification, each pixel is assigned a single ice type. Purple tones indicate various types of YI, including nilas and grey ice (thickness up to 30 cm); yellow and green tones indicate various types of FYI (thickness above 30 cm); brown, orange and red indicate MYI. However, no distinction is made between *thick first-year ice* and *residual ice*, i.e. FYI that has survived the summer melt and has started a new cycle of growth. In the Antarctic, it is relabelled *second-year ice* only after July 1 (JCOMM Expert Team on Sea Ice, 2015; WMO, 2014).

We have compared the weekly SoD charts of the cold seasons of 2017 and 2018 with our ice type data, and also done sporadic comparisons with data from other years. Some examples are presented below. There is an overall correspondence of

https://doi.org/10.5194/tc-2021-381
Preprint. Discussion started: 4 January 2022

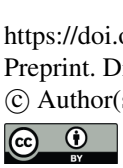

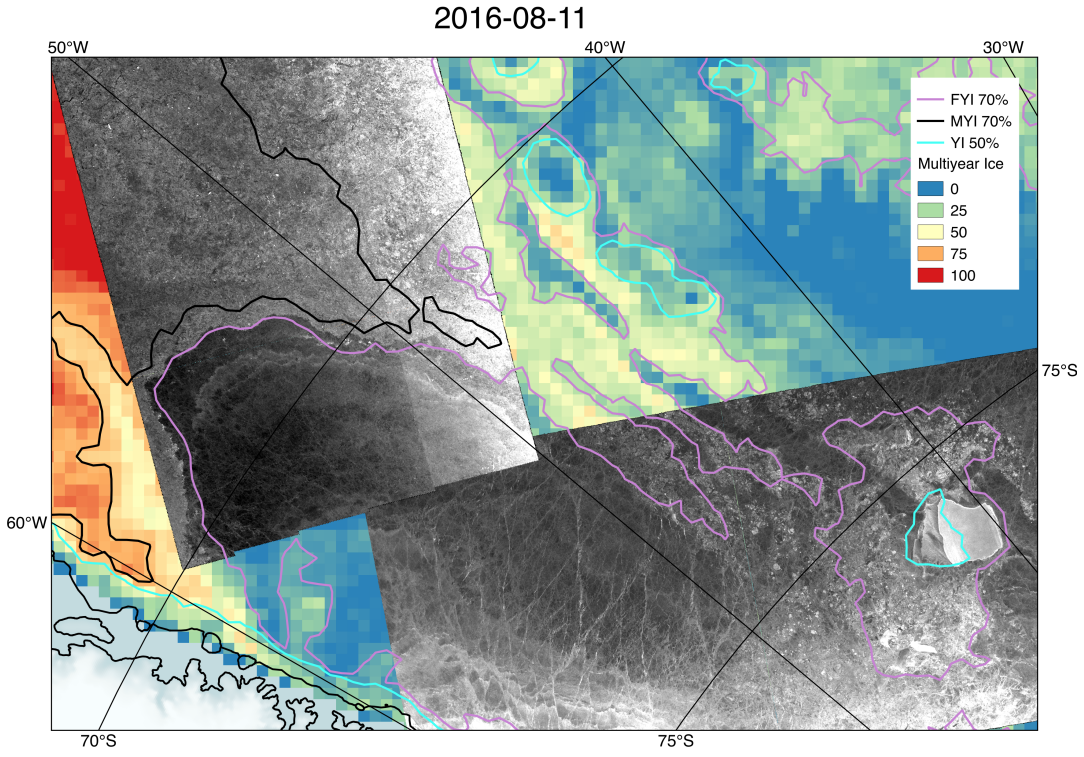

Figure 2. Sentinel-1 SAR image (grey shade) acquired on 11 August, 2016, overlaid on MYI concentration (colour scale) of the same day from ECICE. Dominant ice type from ECICE indicated by contour lines.

the ice types from the charts and the dominant ice type in our data. An example is presented in Figure 3, showing (left to right, top to bottom) the Antarctic SoD chart from AARI (for the week that ends on 30 March, 2017), along with the YI and FYI concentrations from ECICE, and the corrected MYI concentration from ECICE plus correction schemes for 30 March, 2017. The SoD chart has been cropped to save space, the colour legend can be found in the appendix (Table A1). Note the YI (purple tones) in the Eastern Weddell Sea, in the Ross Sea and mainly along the Eastern Antarctic coast. The areas of MYI are in the Western Weddell Sea, in the Amundsen Sea and at the coast of Wilkes Land (130°–170°E). At this early stage of the freezing season, the charts from AARI and from NIC often disagree on the MYI-FYI distinction. As an example Figure 4 shows the Weddell Sea on the same date of 30 March, 2017. The NIC chart (on the right) shows large strips of FYI (yellow) and MYI ("old ice", brown), while the AARI chart (on the left) just shows MYI (and is much closer to the results of our retrieval, see previous figure). From April 2017 on, however, both the AARI and the NIC charts show a large and compact area of MYI in the Weddell Sea (so the strips of FYI marked in yellow in the NIC charts have been re-labelled MYI in brown). A feature that is very well reproduced by the ice type maps in most years is the drifting of the MYI, adjacent to the Ronne Ice Shelf in the inner Weddell Sea at the beginning of the freezing season, towards the North and North-East in the subsequent months, shown for 2017 in Figure 5: The columns show charts and maps of the inner Weddell Sea for 16 March, 27 April, 25 May, and 6

https://doi.org/10.5194/tc-2021-381
Preprint. Discussion started: 4 January 2022

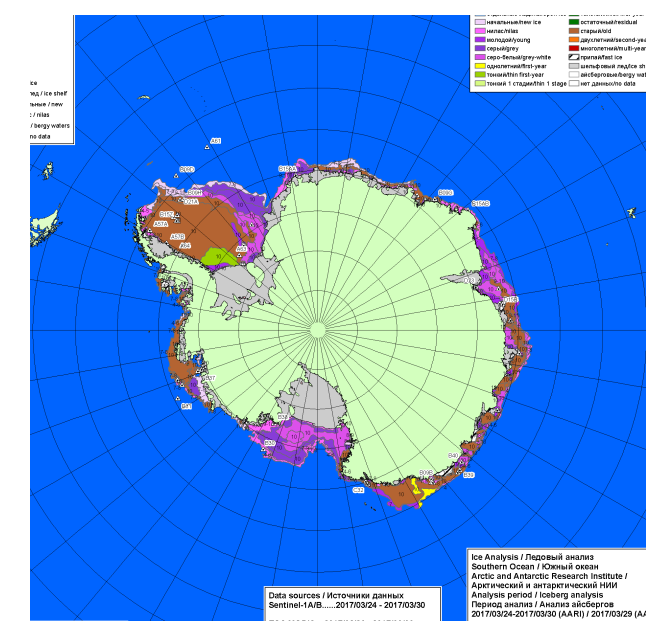

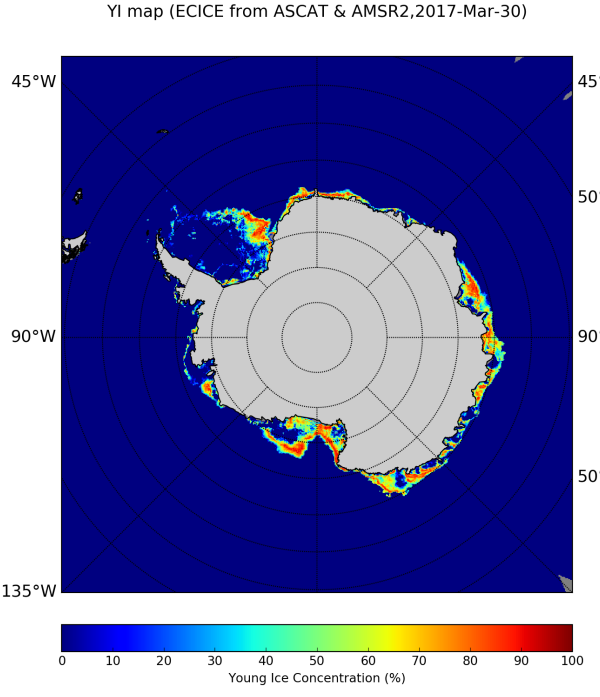

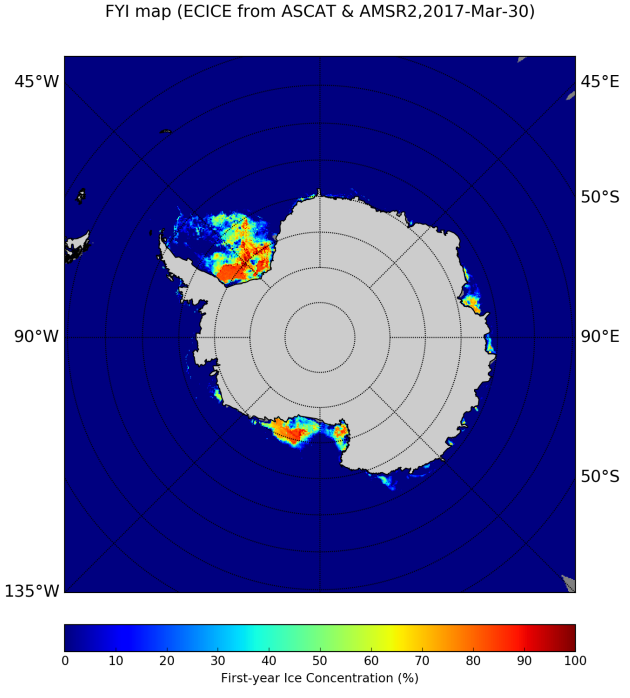

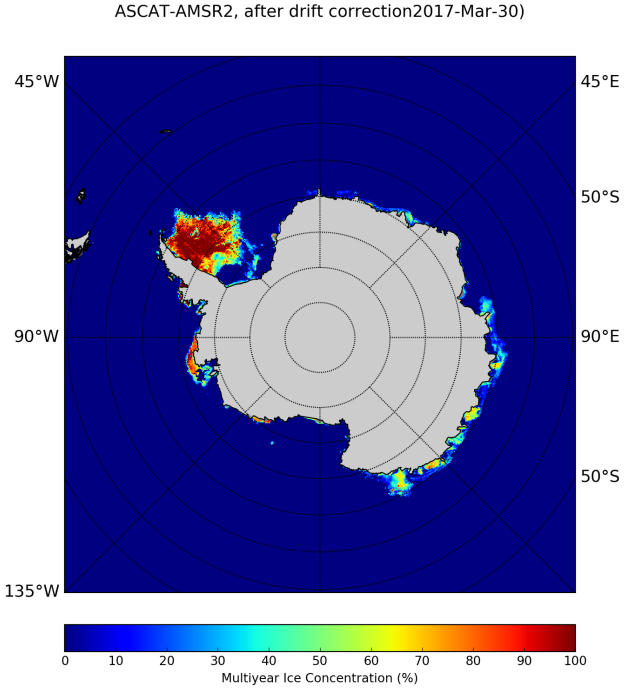

Figure 3. Top left: Stage of Development (SoD) chart by AARI, 30 Mar, 2017; top right: YI concentration (ECICE), bottom left, FYI concentration (ECICE); bottom right: corrected MYI concentration (MYIc, ECICE and correction schemes). In the SoD chart, purple shades are YI (see colour legend in the appendix, Table A1), yellow and green shades are FYI, and brown and orange/red shades are MYI.

https://doi.org/10.5194/tc-2021-381
Preprint. Discussion started: 4 January 2022

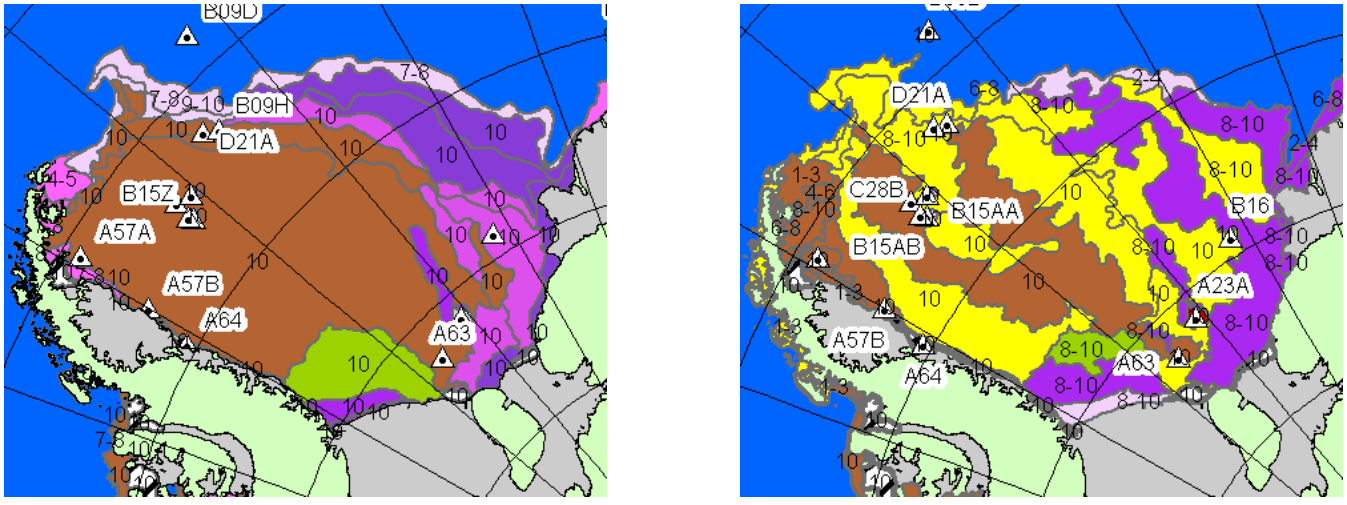

Figure 4. Stage of Development (SoD) charts of the Weddell Sea, 30 March, 2017, from AARI (left) and NIC (right). FYI is yellow, MYI ("old ice") brown (see also colour legend in appendix,Table A1). The triangle symbols denote large icebergs.

July, 2017; namely (top to bottom), SoD, corrected MYI, YI and FYI. The corrected MYI concentration (second row) has a sharp inner (Southern) boundary that agrees well with the boundary between MYI (brown) and YI (purple) or FYI (green and yellow) classes in the SoD charts (top row). The MYI and its inner boundary move towards North and North-East from March to July (left to right). Note the similarity to the FYI-MYI boundary in the previous Section 3.1 (Figure 2), and the two strips of MYI separated by FYI in the right part of the rightmost two SoD charts: The MYI strips correspond to similarly shaped areas with MYI concentration above about 30% to 40% in the MYIc maps (second row). The FYI areas in the SoD maps, in turn, correspond rather to FYI concentrations (forth row) above about 60% to 70%. This hints at the difficulty of comparing a sea ice classification where each point is assigned exactly one sea ice type class with a sea ice type fraction retrieval where in each grid cell, more than one surface type can coexist with the summation of their fractions equal to 100%. The YI and FYI concentration in Figure 5 (third and fourth row) also match reasonably well with the SoD charts, noting that here as well, areas with YI concentration above about 30% correspond to the class YI in the SoD charts, and only FYI concentrations above about 70% correspond to the FYI classes in the SoD charts. This is best visible on the first two maps from the left. Another noteworthy detail are the small patches of YI apparently in the lee of grounded iceberg A23A (third and forth column).

3.3 Polynya Data Set PSSM

A further comparison was made with the already mentioned polynya data based on microwave brightness temperatures from SSM/I (see Section 2.3), from the year 2017, thus avoiding, of course, the data used the probability distribution extraction which where from 2018 (Section 2.3). Figures 6 and 7 are examples of an area in the Ross Sea, near the Ross Ice Shelf, on 3 May and 7 September, 2018, respectively: the left panels of both figures show the map of YI concentration from ECICE; the

https://doi.org/10.5194/tc-2021-381
Preprint. Discussion started: 4 January 2022

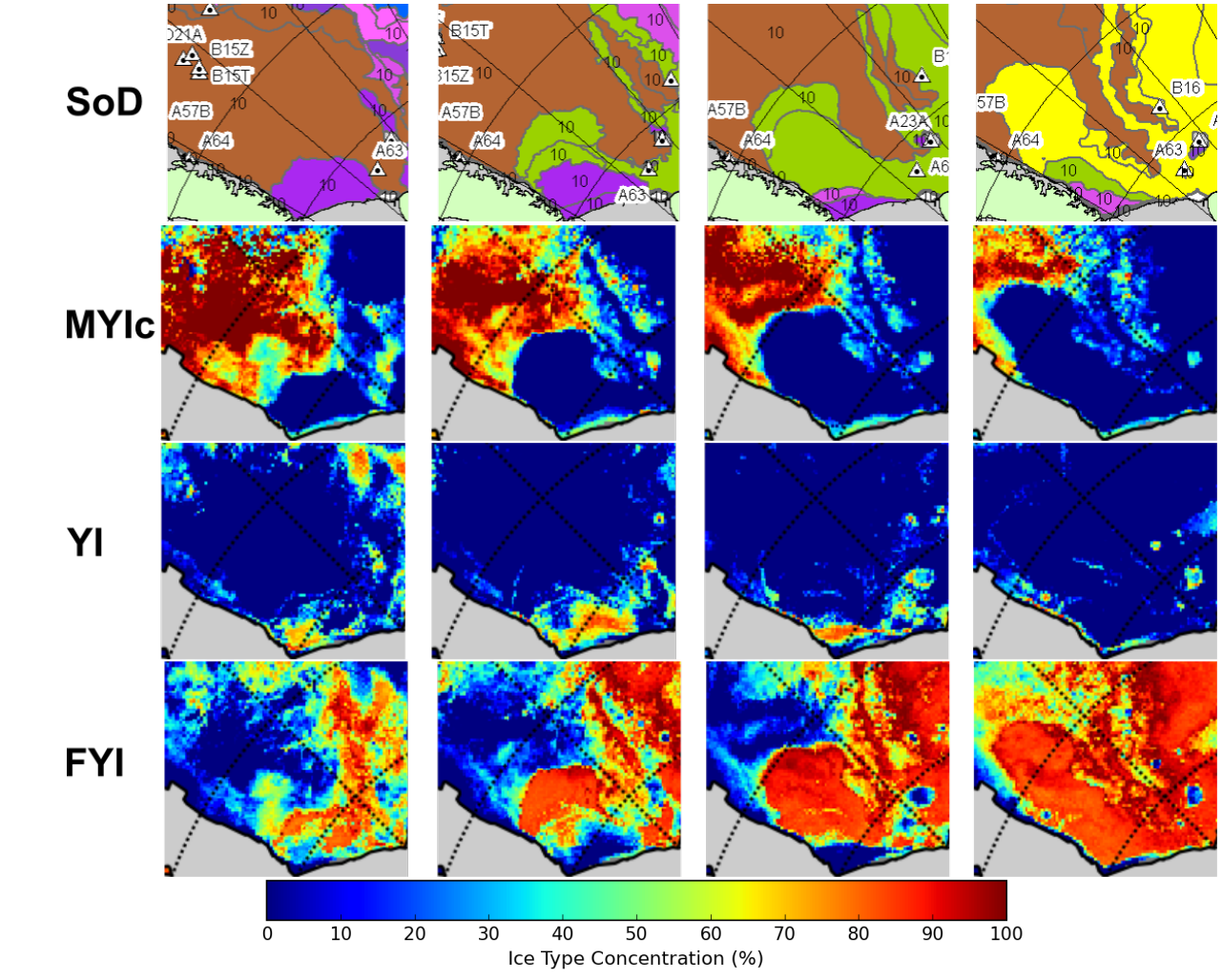

Figure 5. Southwestern Weddell Sea, March to July 2017, top to bottom: SoD chart from AARI, corrected MYI (MYIc), YI, FYI concentration; left to right: 16 March, 27 April, 25 May, 6 July, 2017.

right panels show PSSM maps with the surface type classes open water (dark blue), thin ice (light blue) and other ice (white). The thin ice areas in the polynya data set match the dominantly YI areas from the ECICE retrieval.

Figures 8 and 9 show similar examples from the Weddell Sea, on 2 May, and 19 May, 2017, respectively, demonstrating the variability of coastal polynyas and the young ice associated with them: The thin ice (light blue) in the PSSM maps on the right corresponds roughly to YI concentrations above about 50% (green-yellow-orange) in the retrieved YI maps on the left. On 2 May (Figure 8), there is a large polynya covered with thin ice in the Southwestern Weddell Sea (light blue at the bottom centre of PSSM map on the right) and also coastal polynyas at the Brunt and the Riiser-Larsen Ice Shelves (top right of the PSSM map). Both are matched by high concentrations (orange hues) of YI in the map on the left. On May 19, however

https://doi.org/10.5194/tc-2021-381
Preprint. Discussion started: 4 January 2022

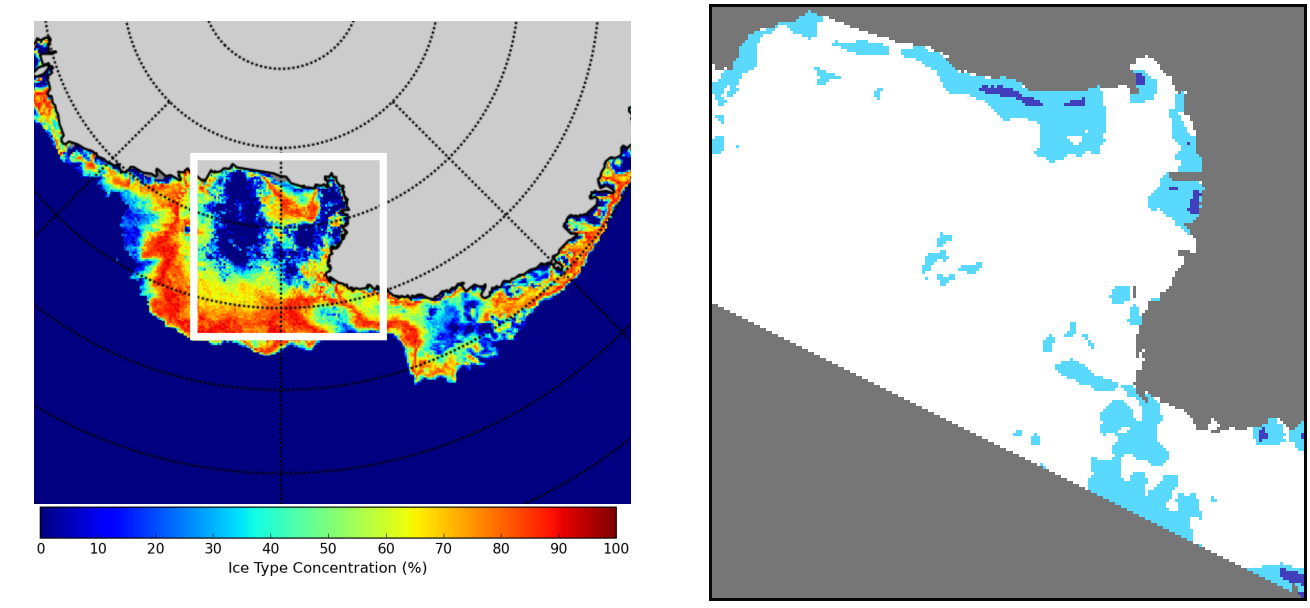

Figure 6. Left: map of YI, 3 May, 2017, right: PSSM polynya map in the area indicated by the white rectangle in the YI map (dark blue: open water, light blue: thin ice, white: other ice).

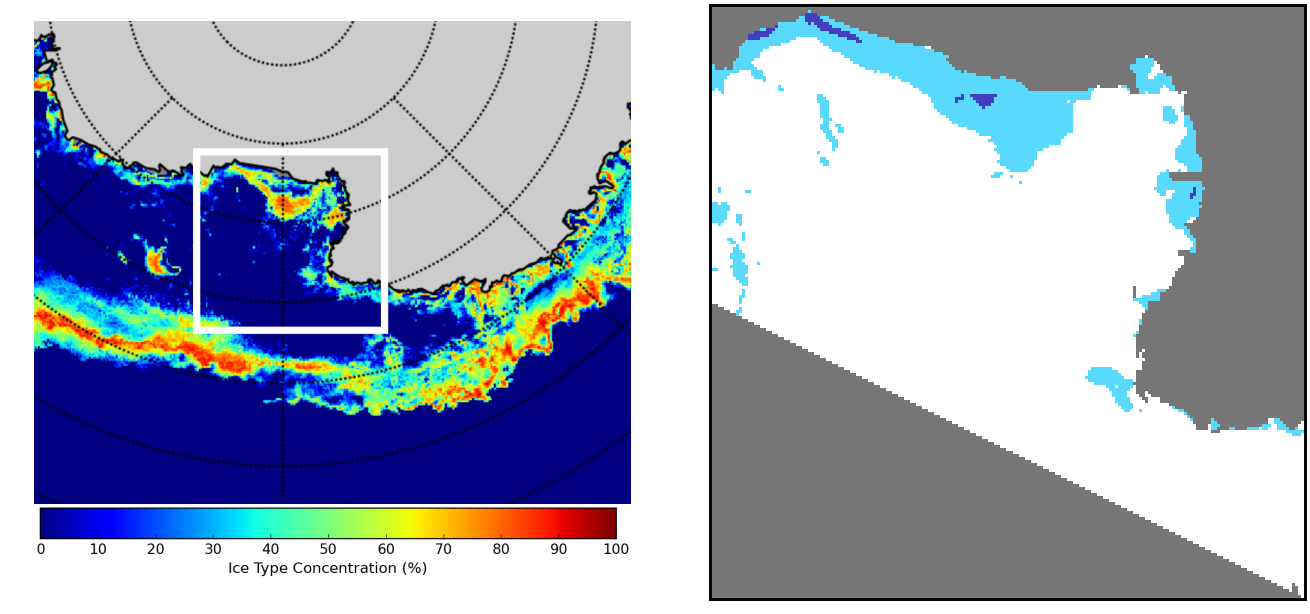

Figure 7. Left: map of YI, 7 Sep., 2017, right: PSSM polynya map in the area indicated by the white rectangle in the YI map (dark blue: open water, light blue: thin ice, white: other ice).

(Figure 9), there is much less polynya activity according to the PSSM map, and also no areas of more than about 40% YI in the map on the left.

https://doi.org/10.5194/tc-2021-381
Preprint. Discussion started: 4 January 2022

The Cryosphere Discussions
Open Access
EGU

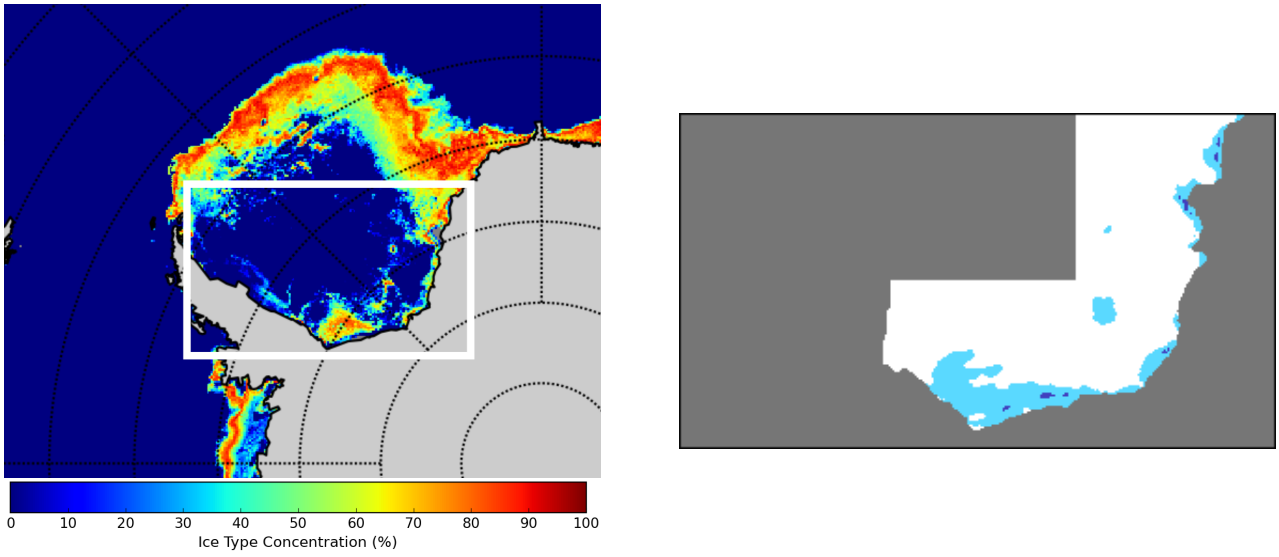

Figure 8. Left: map of YI, 2 May, 2017, right: PSSM polynya map in the area indicated by the white rectangle in the YI map (dark blue: open water, light blue: thin ice, white: other ice).

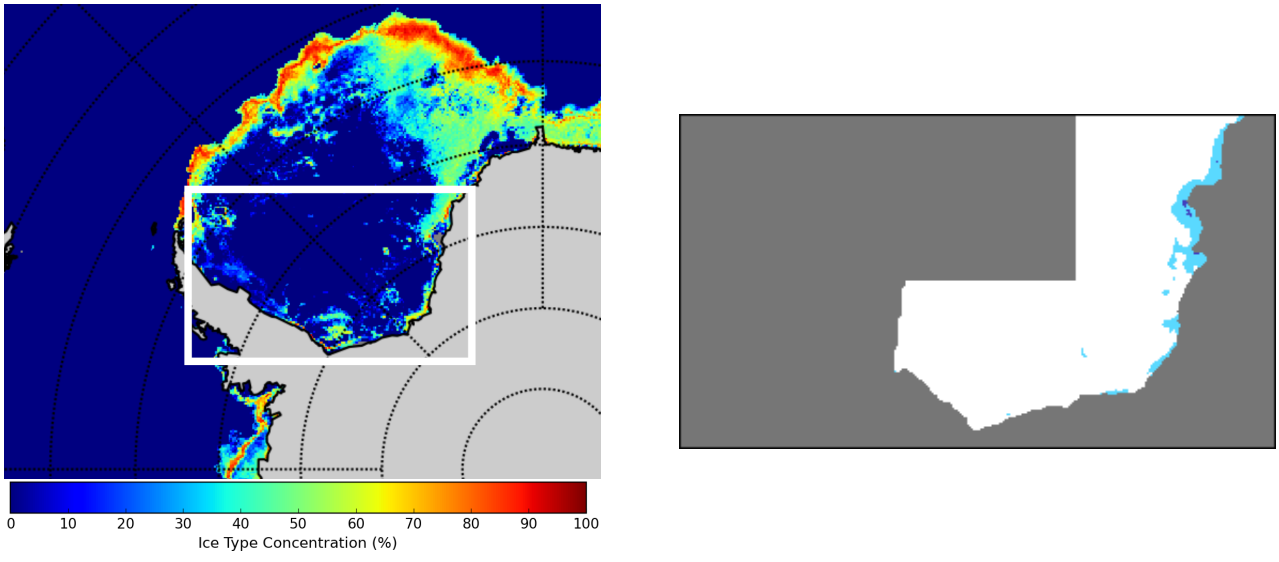

Figure 9. Left: map of YI, 19 May, 2017, right: PSSM polynya map in the area indicated by the white rectangle in the YI map (dark blue: open water, light blue: thin ice, white: other ice).

4 Discussion

As shown in the previous section, the retrieved corrected MYI (MYIc), and also the uncorrected FYI and YI concentrations, compare mostly well with other data, given the limitation that a rigorous validation could not be done yet.

https://doi.org/10.5194/tc-2021-381
Preprint. Discussion started: 4 January 2022

The Cryosphere Discussions
Open Access
EGU

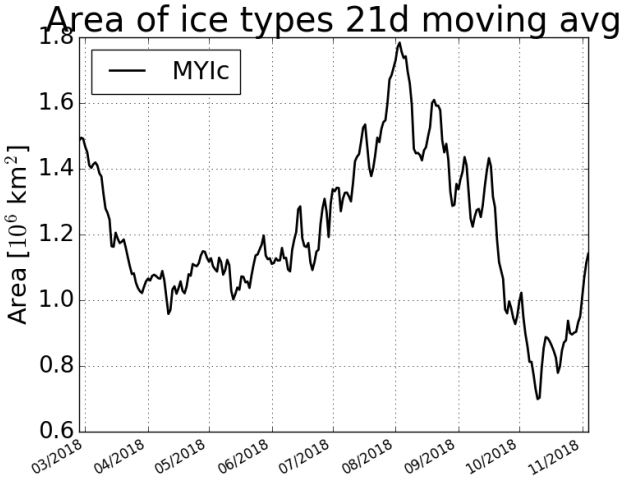

Figure 10. Time series of the total area of corrected MYI in the entire Antarctic, smoothed with a 21 day running mean, March to November 2018.

Large icebergs are often erroneously retrieved as FYI, but this does in principle not cause problems as the position and extent of such icebergs is usually well known and monitored, so they can be masked out using ancillary iceberg data (e.g., https://usicecenter.gov/Products/AntarcIcebergs).

The total area of MYI in the entire Antarctic should not increase during one cold season because MYI originates as the remaining ice at the end of the melting season and hence cannot be generated after freeze-up. However, the total MYI area derived form our data shows large fluctuations, and often an increase around July. This can be seen in Figure 10 which shows the total MYI area for all Antarctic seas for the cold season 2018, smoothed with a 21 day running mean.

The main reason for the increase in July seems to be a large offshore area of MYI in the outer Ross sea and off Wilkes Land, East of the Ross Sea (roughly between 160°E and 140°W, and between 65° and 70°S) that often seems to grow during the cold season and is not eliminated by the drift correction. Figure 11 shows such an area of MYI that appears in late July, 2018, and disappears in September. While, according to the NIC/AARI ice type (SoD) charts, a considerable area of MYI persists far offshore in the outer Ross Sea in many years (though not in the year 2018 shown here), the retrieved offshore MYI areas are larger, in different locations, and sometimes grow quickly within days, which cannot be correct and is not shown on the SoD charts. As MYI cannot be generated during the freezing season, this is clearly spurious identification of MYI. This area of spurious MYI is in the marginal ice zone. A similar phenomenon can be observed at around the same time in that region in all years of the current data record 2013 to 2020 though it is less pronounced in 2019. The most likely reason for this is that in the course of the cold season, the snow layer on FYI in particular in the marginal ice zone changes. Usually, snow backscatter increases and emissivity decreases, making it resemble MYI in that respect. In addition, pancake ice has higher backscatter than FYI and might also be mistaken for MYI (see also Willmes et al., 2011; Arndt et al., 2016; Arndt and Haas, 2019). Elsewhere in the Antarctic seas, such areas of spurious MYI ice can also occur but are generally much smaller. In principle,

https://doi.org/10.5194/tc-2021-381
Preprint. Discussion started: 4 January 2022

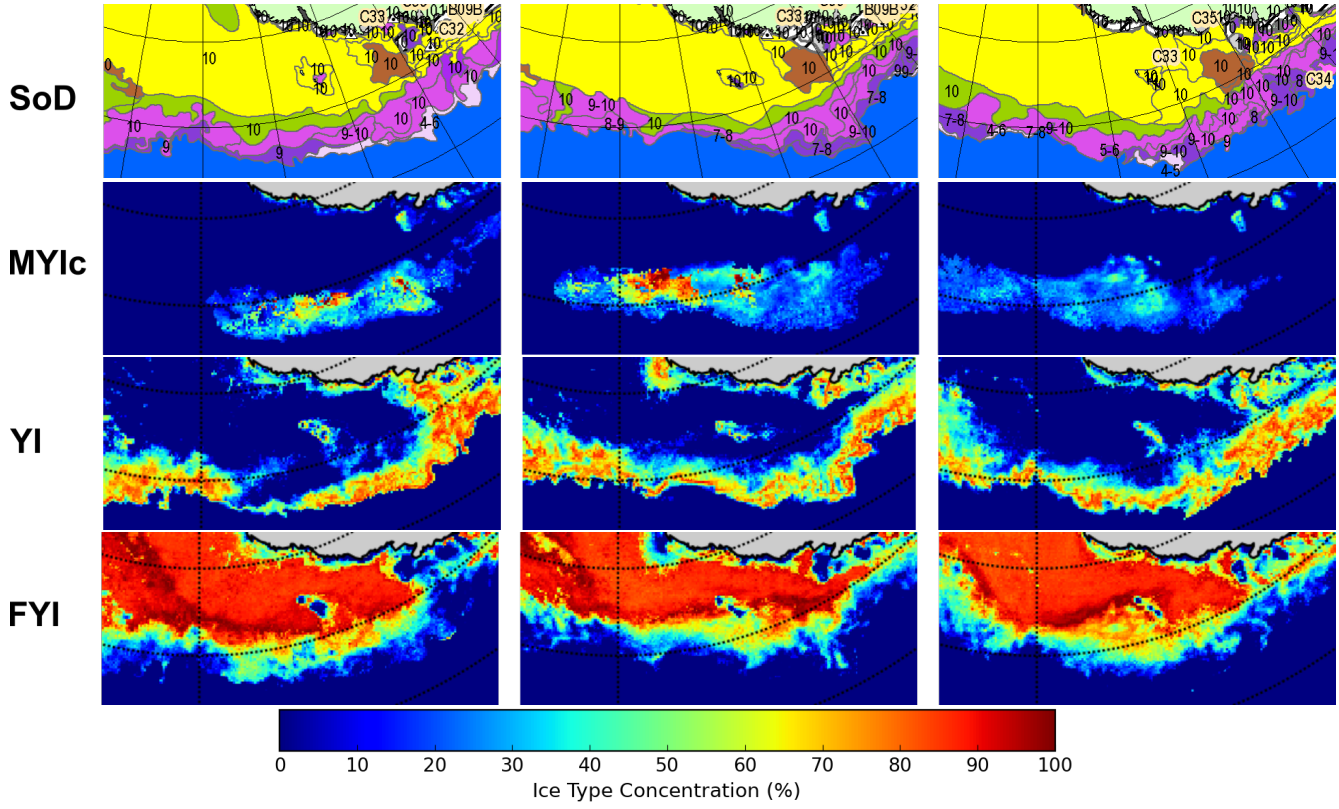

Figure 11. Outer Ross Sea, off Wilkes Land, August and September , 2018, top to bottom: SoD chart from AARI, corrected MYI, YI, FYI concentration; left to right: 2 Aug, 30 Aug, 27 Sep, 2018.

spurious MYI showing up during the cold season should be removed by the drift correction. The fact that this fails can have two possible reasons: (1) problems in the ice drift data used by the drift correction, such as wrong direction or wrong speed - a single drift vector that is much too large can initiate a growing area of spurious MYI (we also add one pixel of uncertainty margin to the drift which might also cause the MYI domain to wrongly extend - cf. Section 2.2.2); (2) single fixed points that permanently, but wrongly show MYI at the beginning of the freezing season, because spurious MYI showing up nearby (within one day's drift) will then not be removed; such seeding points can be caused by "land contamination" of the satellite measurement in footprints directly at the coast or near small islands that are not properly masked. Since removing coastal MYI pixels and extending the land mask before applying the correction had no effect on the spurious MYI pixels, the latter reason can be ruled out. Thus, the reason is most likely inaccuracies in the drift data which accumulate over the season (strange drift vectors have been observed in particular in the Ross sea near the date line; Ted Maksym, priv. comm., 2020).

Instead of trying to correct erroneous MYI, preventing the misclassification that leads to its retrieval in the first place is worth while. To do this, the distributions of MYI and FYI in the different channels, specifically in the outer Ross Sea and off

https://doi.org/10.5194/tc-2021-381
Preprint. Discussion started: 4 January 2022

Wilkes Land, could be investigated. If these distributions differ significantly from those currently used (see Section 2.3), the latter can be adapted.

Towards the end of the freezing season, in September and October, the retrieved, corrected MYI concentration declines strongly in most years (see Figure 10), which is not seen in the weekly SoD charts. However, SoD charts seem to become unstable in the sense that the ice type seems to oscillate between FYI (WMO type 2.5 "first-year ice" (JCOMM Expert Team on Sea Ice, 2015)) and MYI (WMO type 2.6 "old ice") from one week to the next, or from AARI chart to the almost simultaneous NIC chart. The most likely reason for the too strong decline of MYI in our retrieval scheme are temperatures rising to near melting conditions which causes MYI to be misclassified as FYI as described above in Section 2.2.1 about the temperature correction. Since these near-melting or melting conditions are not episodic any more, they cannot be corrected by the temperature correction.

Note that a first analysis of the new OSI-SAF ice type classification data likewise does not show the expected decrease of Antarctic MYI area in the course of the season, but instead a steady slow increase followed by a rapid decline toward the end of the freezing season in September/October (Aaboe et al., 2021b, Fig. 14), which is similar to the time series derived from our data (Figure 10).

5 Summary and Conclusions

The sea ice type retrieval method ECICE (Shokr et al., 2008; Shokr and Agnew, 2013) and the subsequent correction schemes for MYI (Ye et al., 2016a, b) developed for the Arctic can be adapted for the Antarctic, given samples of Antarctic ice types. Input satellite data are microwave radiances at several channels as well as scatterometer backscattering measurements. Daily maps of uncorrected YI, FYI and MYI, and of MYI corrected for effects of melt-refreeze and snow metamorphosis, can be retrieved, outside the melt season, at spatial resolution of 12.5 km. The results look reasonable in the sense that they show agreement with SAR images, with remote-sensing-based polynya data, and with weekly charted sea ice stage of development (so far the only source of ice type information in the Antarctic). In particular, the general distribution of the Antarctic MYI at the beginning of the freezing season is well captured. The subsequent time evolution of the MYI concentration in the Weddell Sea, as far as the AARI/NIC stage of the development charts can tell, is captured as well in the months after freeze-up, showing the effects of advection and melt. The retrieved distributions of YI and FYI concentration are reasonable as well. However, comparing our ice type concentrations, i.e., area fractions of ice types, with weekly charts that assign only one ice type to each location is inherently problematic. A more detailed validation study that also includes in-situ observations from research cruises is planned. The most problematic area is the outer Ross Sea and the sea off Wilkes Land, where large and growing areas of spurious MYI are retrieved in the marginal ice zone in late winter in most years. The data become unstable toward the end of the freezing season in September/October, with MYI being underestimated. The new time series, spanning the years 2013 to 2020, is the first comprehensive time series to give insight into the distribution and evolution of Antarctic sea ice types, which outweighs the shortcomings that still exist. The current time series of uncorrected YI, FYI, MYI and MYIc can be extended backwards to 2002. The time series can be continued for the years to come, as the successor instrument of the radiometer

https://doi.org/10.5194/tc-2021-381
Preprint. Discussion started: 4 January 2022

Colour		RGB colour model	Stage of development (SoD)	Number from WMO Sea Ice Nomenclature
alternative	prime			
		000-100-255	Ice free	4.2.8
		150-200-255	<1/10 ice of unspecified SoD (open water)	4.2.6
		240-210-250	New ice	2.1
		255-175-255	Dark nilas	2.2.1
		255-100-255	Light nilas	2.2.2
		170-040-240	Young ice	2.4
		135-060-215	Grey ice	2.4.1
		220-080-235	Grey-white ice	2.4.2
		255-255-000	First-year ice (FY)	2.5
		155-210-000	FY thin ice (white ice)	2.5.1
		215-250-130	FY thin ice (white ice) first stage	2.5.1.1
		175-250-000	FY thin ice (white ice) second stage	2.5.1.2
		000-200-020	FY medium ice	2.5.2
		000-120-000	FY thick ice	2.5.3
		180-100-050	Old ice	2.6
		000-120-000	Residual ice	2.6.1
		255-120-010	Second-year ice	2.6.2
		200-000-000	Multi-year ice	2.6.3

Table A1. Colour coding of the sea ice types in the ice charts shown above

AMSR2, namely, AMSR3, is scheduled for launch in the next few years, and scatterometers will be on the future MetOp satellites. In addition, there is the new Chinese-French Oceanography Satellite (CFO-Sat) carrying a K_u band scatterometer, and the upcoming mission CIMR (Copernicus Imaging Microwave Radiometer, see Kilic et al., 2018) with radiometer channels from 1.4 to 36.5 GHz, that might even enable sea ice type retrieval without additional scatterometer data.

Data availability. The uncorrected sea ice type data of the Antarctic, years 2013 to present, are available at the web site http://seaice.uni-bremen.de; the corrected MYI data of the Antarctic, years 2013-2019, are available on the same web site, and, in addition, as a data set in the PANGAEA archive, https://doi.org/10.1594/PANGAEA.909054

Appendix A: WMO colour coding of sea ice types

The AARI/NIC ice charts showing the stage of development in Figures 3 to 11 use the colour code specified by WMO (2014). For easier reference, the colour codes of the ice types relevant here are shown in Table A1.

Author contributions. CM has adapted the algorithm and correction schemes for the Antarctic and wrote the initial manuscript; YY has developed the original correction schemes for the Arctic and has given feedback and advice for the work; MS has contributed the original

https://doi.org/10.5194/tc-2021-381
Preprint. Discussion started: 4 January 2022

ECICE retrieval which is the basis of the whole retrieval and has given important feedback and advice; GS has contributed the comparison with SAR data, and has given critical scientific advice in all stages of the work; all co-authors have reviewed the manuscript.

Competing interests. The authors declare that they have no competing interests.

Acknowledgements. This work was supported by the Deutsche Forschungsgemeinschaft (DFG), project SITAnt, grant SP1128/2-1, in the framework of the Antarctic priority programme SPP 1158 "Antarctic Research with comparative investigations in Arctic ice areas". The authors acknowledge the International Space Science Institute (ISSI) in Bern for support and for discussions in the ISSI team "Satellite-Derived Estimates of Antarctic Snow and Ice Thickness" led by P. Heil, University of Tasmania. The authors are very grateful to S. Kern, University of Hamburg, for producing and providing the polynya data set, and to S. Arndt and C. Haas, Alfred Wegener Institute, Bremerhaven, for important discussions.

https://doi.org/10.5194/tc-2021-381
Preprint. Discussion started: 4 January 2022

References

Aaboe, S., Down, E. J., and Eastwood, S.: Algorithm Theoretical Basis Document for the Global Sea-Ice Edge and Type Product, Version 3.3, Tech. rep., EUMETSAT Ocean and Sea Ice SAF, https://osisaf-hl.met.no/sites/osisaf-hl.met.no/files/baseline_document/osisaf_cdop3_ss2_atbd_sea-ice-edge-type_v3p3.pdf, 2021a.

Aaboe, S., Down, E. J., and Eastwood, S.: Validation Report for the Global Sea-Ice Edge and Type Product, Version 3.1, Tech. rep., EUMETSAT Ocean and Sea Ice SAF, https://osisaf-hl.met.no/sites/osisaf-hl.met.no/files/validation_reports/osisaf_cdop3_ss2_svr_sea-ice-edge-type_v3p1.pdf, 2021b.

Arndt, S. and Haas, C.: Spatiotemporal variability and decadal trends of snowmelt processes on Antarctic sea ice observed by satellite scatterometers, The Cryosph., 13, 1943–1958, https://doi.org/10.5194/tc-13-1943-2019, 2019.

Arndt, S., Willmes, S., Dierking, W., and Nicolaus, M.: Timing and regional patterns of snowmelt on Antarctic sea ice from passive microwave satellite observations, J. Geophys. Res. Oceans, 121, 5916–5930, https://doi.org/10.1002/2015JC011504, 2016.

Comiso, J. C.: Large Decadal Decline of the Arctic Multiyear Ice Cover, Journal of Climate, 25, 1176–1193, https://doi.org/10.1175/jcli-d-11-00113.1, 2012.

Dee, D. P.: The ERA-Interim reanalysis: Configuration and performance of the data assimilation system, Q. J. Roy. Meteor. Soc., 137, 553–597, https://doi.org/10.1002/qj.828, 2011.

Drobot, S. D. and Anderson, M. R.: An improved method for determining snowmelt onset dates over Arctic sea ice using scanning multichannel microwave radiometer and Special Sensor Microwave/Imager data, J. Geophys. Res., 106, 24 033–24 049, https://doi.org/10.1029/2000JD000171, 2001.

Haas, C., Thomas, D. N., and Bareiss, J.: Surface properties and processes of perennial Antarctic sea ice in summer, Journal of Glaciology, 47, 613–625, https://doi.org/10.3189/172756501781831864, 2001.

Hobbs, W. R., Bindoff, N. L., and Raphael, M. N.: New Perspectives on Observed and Simulated Antarctic Sea Ice Extent Trends Using Optimal Fingerprinting Techniques, J. Clim., 28, 1543–1560, https://doi.org/10.1175/JCLI-D-14-00367.1, 2015.

JCOMM Expert Team on Sea Ice: WMO Sea Ice Nomenclature, volumes I, II, and II (WMO-259), Tech. rep., World Meteorological Organization, https://jcomm.info/index.php?option=com_oe&task=viewDocumentRecord&docID=14598, 2015.

Johannessen, O. M., Shalina, E. V., and Miles, M. W.: Satellite Evidence for an Arctic Sea Ice Cover in Transformation, Science, 286, 1937–1939, https://doi.org/10.1126/science.286.5446.1937, 1999.

Kern, S., Spreen, G., Kaleschke, L., De La Rosa, S., and Heygster, G.: Polynya Signature Simulation Method polynya area in comparison to AMSR-E 89GHz sea-ice concentrations in the Ross Sea and off the Adélie Coast, Antarctica, for 2002: first results, Ann. Glaciol., 46, 409–418, https://doi.org/10.3189/172756407782871585, 2007.

Kilic, L., Prigent, C., Aires, F., Boutin, J., Heygster, G., Tonboe, R. T., Roquet, H., Jimenez, C., and Donlon, C.: Expected Performances of the Copernicus Imaging Microwave Radiometer (CIMR) for an All-Weather and High Spatial Resolution Estimation of Ocean and Sea Ice Parameters, J. Geophys. Res. Oceans, 123, 7564–7580, https://doi.org/10.1029/2018JC014408, 2018.

Kwok, R., Cunningham, G., Wensnahan, M., Rigor, I., Zwally, H., and Yi, D.: Thinning and volume loss of Arctic sea ice: 2003–2008, J. Geophys. Res., 114, C07005, https://doi.org/10.1029/2009JC005312, 2009.

Lavergne, T., Eastwood, S., Teffah, Z., Schyberg, H., and Breivik, L.-A.: Sea ice motion from low resolution satellite sensors: an alternative method and its validation in the Arctic, J. Geophys. Res., 115, C10032, https://doi.org/10.1029/2009JC005958, 2010.

https://doi.org/10.5194/tc-2021-381
Preprint. Discussion started: 4 January 2022

Ludescher, J., Yuan, N., and Bunde, A.: Detecting the statistical significance of the trends in the Antarctic sea ice extent: an indication for a turning point, Climate Dynamics, 53, 237–244, https://doi.org/10.1007/s00382-018-4579-3, 2019.

Mahlstein, I., Gent, P. R., and Solomon, S.: Historical Antarctic mean sea ice area, sea ice trends, and winds in CMIP5 simulations, J. Geophys. Res., 118, 5105–5110, https://doi.org/10.1002/jgrd.50443, 2013.

Markus, T. and Burns, B. A.: A method to estimate subpixel-scale coastal polynyas with satellite passive microwave data, J. Geophys. Res. Oceans, 100, 4473–4487, https://doi.org/10.1029/94JC02278, 1995.

Massom, R. A. and Stammerjohn, S. E.: Antarctic sea ice change and variability – Physical and ecological implications, Polar Science, 4, 149–186, https://doi.org/10.1016/j.polar.2010.05.001, antarctic Biology in the 21st Century - Advances in and beyond IPY, 2010.

Melsheimer, C. and Spreen, G.: IUP Multiyear Ice Concentration and other sea ice types, Version 1.1 (Arctic)/Version AQ2 (Antarctic) – User Guide, Tech. rep., Institute of Environmental Physics, University of Bremen, https://seaice.uni-bremen.de/data/MultiYearIce/MYIuserguide.pdf, accessed: 2020-04-07, 2019.

Melsheimer, C. and Spreen, G.: AMSR2 ASI sea ice concentration data, Antarctic, version 5.4 (NetCDF) (July 2012 - December 2019), https://doi.org/10.1594/PANGAEA.898400, 2019.

Meredith, M., Sommerkorn, M., Cassotta, S., Derksen, C., Ekaykin, A., Hollowed, A., Kofinas, G., Mackintosh, A., Melbourne-Thomas, J., Muelbert, M., Ottersen, G., Pritchard, H., and Schuur, E.: Polar Regions, in: IPCC Special Report on the Ocean and Cryosphere in a Changing Climate, edited by Pörtner, H.-O., Roberts, D., Masson-Delmotte, V., Zhai, P., Tignor, M., Poloczanska, E., Mintenbeck, K., Alegría, A., Nicolai, M., Okem, A., Petzold, J., Rama, B., and Weyer, N., IPCC, https://www.ipcc.ch/srocc/chapter/chapter-3-2/, in press, 2019.

Nihashi, S. and Ohshima, K. I.: Circumpolar Mapping of Antarctic Coastal Polynyas and Landfast Sea Ice: Relationship and Variability, J. Clim., 28, 3650–3670, https://doi.org/10.1175/JCLI-D-14-00369.1, 2015.

Parkinson, C. L.: A 40-y record reveals gradual Antarctic sea ice increases followed by decreases at rates far exceeding the rates seen in the Arctic, Proc. Natl. Acad. Sci. USA, 116, 14 414–14 423, https://doi.org/10.1073/pnas.1906556116, 2019.

Parkinson, C. L. and Cavalieri, D. J.: Antarctic sea ice variability and trends, 1979–2010, The Cryosphere, 6, 871–880, https://doi.org/10.5194/tc-6-871-2012, 2012a.

Parkinson, C. L. and Cavalieri, D. J.: Arctic sea ice variability and trends, 1979–2010, The Cryosphere, 6, 881–889, https://doi.org/10.5194/tc-6-881-2012, 2012b.

Polvani, L. M. and Smith, K. L.: Can natural variability explain observed Antarctic sea ice trends? New modeling evidence from CMIP5, Geophys. Res. Lett., 40, 3195–3199, https://doi.org/10.1002/grl.50578, 2013.

Shokr, M. and Agnew, T. A.: Validation and potential applications of Environment Canada Ice Concentration Extractor (ECICE) algorithm to Arctic ice by combining AMSR-E and QuikSCAT observations, Remote Sens. Environ., 128, 315–332, https://doi.org/10.1016/j.rse.2012.10.016, 2013.

Shokr, M., Lambe, A., and Agnew, T.: A New Algorithm (ECICE) to Estimate Ice Concentration From Remote Sensing Observations: An Application to 85-GHz Passive Microwave Data, IEEE Trans. Geosci. Remote Sens., 46, 4104–4121, https://doi.org/10.1109/tgrs.2008.2000624, 2008.

Spreen, G., Kaleschke, L., and Heygster, G.: Sea Ice Remote Sensing Using AMSR-E 89 GHz Channels, J. Geophys. Res., 113, C02S03, https://doi.org/10.1029/2005JC003384, 2008.

Stocker, T., Qin, D., Plattner, G.-K., Tignor, M., Allen, S., Boschung, J., Nauels, A., Xia, Y., Bex, V., and Midgley, P., eds.: Climate Change 2013: The Physical Science Basis. Contribution of Working Group I to the Fifth Assessment Report of the In-

tergovernmental Panel on Climate Change, Cambridge University Press, Cambridge, United Kingdom and New York, NY, USA, https://doi.org/10.1017/CBO9781107415324, 2013.

Tschudi, M., Fowler, C., Maslanik, J., Stewart, J. S., and Meier, W.: EASE-Grid Sea Ice Age, https://doi.org/10.5067/PFSVFZA9Y85G, accessed: 2017-09-01, 2016.

Turner, J., Hosking, J. S., Bracegirdle, T. J., Marshall, G. J., and Phillips, T.: Recent changes in Antarctic Sea Ice, Phil. Trans. R. Soc. A, 373, 20140163, https://doi.org/10.1098/rsta.2014.0163, 2015.

Willmes, S., Haas, C., and Nicolaus, M.: High radar-backscatter regions on Antarctic sea-ice and their relation to sea-ice and snow properties and meteorological conditions, Int. J. Remote Sens., 32, 3967–3984, https://doi.org/10.1080/01431161003801344, 2011.

WMO: Ice Chart Colour Code Standard, May 2014 edition (revision 1), Tech. rep., World Meteorological Organization, https://jcomm.info/index.php?option=com_oe&task=viewDocumentRecord&docID=4914, 2014.

Ye, Y., Heygster, G., and Shokr, M.: Improving Multiyear Ice Concentration Estimates With Reanalysis Air Temperatures, IEEE Trans. Geosci. Remote Sens., 54, 2602–2614, https://doi.org/10.1109/tgrs.2015.2503884, 2016a.

Ye, Y., Shokr, M., Heygster, G., and Spreen, G.: Improving Multiyear Sea Ice Concentration Estimates with Sea Ice Drift, Remote Sensing, 8, 397, https://doi.org/10.3390/rs8050397, 2016b.

Ye, Y., Shokr, M., Aaboe, S., Aldenhoff, W., Eriksson, E. B. L., Heygster, G., Melsheimer, C., and Girard-Ardhuin, F.: Inter-comparison and evaluation of sea ice type concentration algorithms, The Cryosph. Disc., https://doi.org/10.5194/tc-2019-200, 2019.

Zunz, V., Goosse, H., and Massonnet, F.: How does internal variability influence the ability of CMIP5 models to reproduce the recent trend in Southern Ocean sea ice extent?, The Cryosph., 7, 451–468, https://doi.org/10.5194/tc-7-451-2013, 2013.